

## MOLECULAR BIOLOGY

# Multiplexing light-inducible recombinases to control cell fate, Boolean logic, and cell patterning in mammalian cells

Cristina Tous, Ian S. Kinstlinger, Maya E. L. Rice, Jenny Deng, Wilson W. Wong\*

Light-inducible regulatory proteins are powerful tools to interrogate fundamental mechanisms driving cellular behavior. In particular, genetically encoded photosensory domains fused to split proteins can tightly modulate protein activity and gene expression. While light-inducible split protein systems have performed well individually, few multichromatic and orthogonal gene regulation systems exist in mammalian cells. The design space for multichromatic circuits is limited by the small number of orthogonally addressable optogenetic switches and the types of effectors that can be actuated by them. We developed a library of red light-inducible recombinases and directed patterned myogenesis in a mesenchymal fibroblast-like cell line. To address the limited number of light-inducible domains (LIDs) responding to unique excitation spectra, we multiplexed light-inducible recombinases with our “Boolean logic and arithmetic through DNA excision” (BLADE) platform. Multiplexed optogenetic tools will be transformative for understanding the role of multiple interacting genes and their spatial context in endogenous signaling networks.

## INTRODUCTION

The ability to optogenetically control transgene expression has revolutionized our ability to understand cellular signaling. Light can rapidly perturb a protein with high spatiotemporal control (1, 2), which is invaluable for mapping the effect of specific genetic regulation onto downstream cell state changes (1, 3, 4). For example, optical stimulation of channelrhodopsin-2 has been used to delineate sleep state transitions (5), motor cortex function (6), and fear memory recall (7). In comparison to light, chemical inducers traditionally used to control genetic circuits diffuse freely, thwarting the possibility to pattern gene expression (8). While there are many examples of optogenetics transiently modulating cells (9, 10), there is a lack of tools to permanently perturb a cell, especially beyond the more heavily explored blue wavelengths. Biological processes are governed by a network of genes dynamic in both space and time, necessitating multiwavelength control. In the context of skeletal muscle models in mice, fibrosis is affected by the spatiotemporal expression of various genes (Vim, Fn1, and ThbS4), as is regeneration (MyoD, Myl4, Hsp2, and Sparc) and calcification (Bgn, Ctsk, and Spp1) (11). Multiwavelength controllable gene circuits will ultimately pave the way for more precise disease and regeneration models critical to understanding the molecular mechanisms underlying cell signaling in those contexts.

Optogenetics takes advantage of photosensitive proteins that can be genetically encoded to offer a layer of light-inducible regulation. Pioneers of the field leveraged opsins, which have traditionally controlled ion flow in neurons, to elicit desired biological responses (1, 12, 13). A complementary approach involves engineering pairs of dimerization-based optogenetic switches to control the activity of gene editing tools (2, 14). Focusing on the latter approach, investigators have developed a vast collection of blue light–dimerization tools using light-oxygen-voltage domains (15, 16) and cryptochromes (17, 18), which are responsive to blue light (19). In addition to blue light domains, investigators have identified and modified red light

domains leveraging the red light–specific affinity of Phytochromes (20). Red light penetrates tissues deeper than blue light because longer wavelengths result in less scattering and absorption than shorter wavelengths (20, 21). By splitting a protein and fusing light responsive domains, researchers have created many unique switches using recombinases (22, 23), transcription factors (21, 24–26), and Cas proteins (27, 28).

Now, there is an untapped opportunity to multiplex wavelengths, where multiple cell perturbations are controlled independently by light. Orthogonally controlled tools would open the possibility of creating logic-encoded gene circuits and increase the complexity exerted over synthetic circuits. Previous studies have established the possibility of orthogonally controlling genes in the same cell. However, they have not demonstrated Boolean-encoded logic, multichromatic patterning, or permanent control over gene outputs.

Two published multichromatic systems multiplexed three light-inducible transcription factors to control the expression of three independent outputs. In the first study, two heterodimerizing transcription factors responsive to ultraviolet light (311 nm) and red light (660 nm) were multiplexed with a homodimerizing blue light–inducible (465 nm) transcription factor (29). More recently, a bidirectional, cyanobacteriochrome-based light-inducible dimer (BICYCL) system was engineered to respond to red (660 nm) and green (525 nm) light (30). In addition to developing binders to Amg2, this study multiplexed red, green, and blue (455 nm) heterodimerizing transcription factors. Another innovative multichromatic system was developed using blue (450 nm) light–inducible optoAKT1 and red/far-red (660/740 nm) light–inducible optoSOS to control orthogonal cellular signaling pathways (31).

While these studies demonstrate proof-of-concept multiplexing of light-inducible gene regulation tools, they have a few drawbacks. First, they require continuous illumination for sustained perturbation. Second, without incorporating Boolean logic—which is challenging with transcription factors and signaling cascades—those circuits can only control one output per wavelength. Last, there is an absence of gene patterning in two of the three above-mentioned multichromatic circuits and no instances of orthogonally patterned

Copyright © 2025 The Authors, some rights reserved; exclusive licensee American Association for the Advancement of Science. No claim to original U.S. Government Works. Distributed under a Creative Commons Attribution NonCommercial License 4.0 (CC BY-NC).

Department of Biomedical Engineering, Biological Design Center, Boston University, Boston, MA 02215, USA.

\*Corresponding author. Email: wilwong@bu.edu

outputs or logic-encoded outputs. There is an urgent need for more gene regulatory tools that enable precise multiplex and programmable control. Expanding the synthetic biologist's toolbox to include light-inducible recombinases will broaden our spatiotemporal regulatory control to DNA modification, which we can leverage to perform more complex computations than transcriptional regulation-based systems. There is additionally a need to spatially control gene editing to enable the creation of higher-order tissue functions because spatially organized gene expression is a requirement for more complex tissue function. Together, these advancements will push the boundaries of synthetic biology to augment the complexity of circuits possible to ultimately understand the spatial dynamics of biological systems and to apply spatial control toward applications in regeneration and cell modeling.

Existing multichromatic circuits take advantage of transcription factors and kinases, which require continuous illumination for sustained perturbation. Permanent optogenetic switches would alleviate the need to continuously illuminate cells to achieve sustained perturbation or gene expression, which may be important for applications in disease (32, 33) and cell fate pathway modeling (34, 35). Site-specific recombinases (SSRs) are an important class of tools that can permanently delete, insert, or reconfigure parts of DNA with high fidelity (36, 37). This is advantageous within optogenetics because a single illumination dose is sufficient to permanently activate or repress gene expression. In comparison, transcription factors transiently modify gene expression and require repeat illumination doses to maintain perturbation, expression, or repression. In contrast, the irreversibility of Cre editing makes it especially important to reduce dark activity. Despite this problem, there is an existing blue light-inducible (470 nm) Cre *in vivo* model that does not suffer from a prohibitive amount of dark activity (23).

Although light-inducible recombinases have been used under the control of one wavelength (22, 23, 38), they have yet to be multiplexed. Multiplexing recombinases opens the opportunity to engineer cells to perform computations (for example, AND, OR, NOT logic) and execute precise biological functions. Promising multiplexing platforms for recombinases include ConVERGD (conditional viral expression by ribozyme guided degradation) (39), INTRSECT (intronic recombinase sites enabling combinatorial targeting) (40), and BLADE (Boolean logic and arithmetic through DNA excision). Of these platforms, BLADE is the only architecture that unlocks the opportunity to have an exponential increase in outputs. With BLADE, orthogonal recombinases execute Boolean logic by performing excision at cognate recognition sites on a single transcriptional unit, which has been leveraged with chemical-inducible recombinases. Instead of having 1:1 inputs to outputs with single reporter circuits, two recombinase inputs multiplexed with BLADE yields four outputs, and three inputs yields eight outputs. In the previously mentioned multichromatic circuits, the number of independent outputs can never be higher than the number of LID-responsive excitation spectra. Boolean logic is one way to circumvent the challenge of a limited number of orthogonal light-inducible domains (LIDs). One of the greatest advantages of recombinases is the potential to encode sophisticated logic to control multiple outputs within a cell (41–43).

In this paper, we describe the largest collection of red light-inducible recombinases to date. We present 10 red light-inducible recombinases, and we showcase the potential of these tools by patterning a red light-inducible myogenesis switch that turns on MyoD and converts fibroblasts to myotubes. This collection also opens the

opportunity for multiplexing logic-based circuits. We select the highest performing red light-inducible recombinases to test in a pairwise screen with blue light-inducible recombinases to carry out AND gate logic. From this screen, we identify three red light Flp and blue light Cre pairs with fold changes over 10. We further test orthogonality with our laboratory's previously introduced two-input–four-output BLADE (Boolean logic and arithmetic through DNA excision) decoder and show that we could reproduce BLADE decoder logic with optical rather than genetic or chemical inputs. Last, we spatially pattern orthogonal gene outputs within mammalian cells. We expect that the multiplexed optogenetic tools described here will be transformative for understanding the role of multiple interacting genes in endogenous signaling networks.

## RESULTS

### Library of red light-inducible recombinases

Although many laboratories have designed high-performing blue light-inducible recombinases to control gene switches *in vitro* and *in vivo* (19, 23, 44), there exists no corresponding library of red light-inducible recombinases. To design red light-inducible recombinases, we fused three previously identified candidate red light responsive dimerization domains (Fig. 1A) to five different split Cre recombinases. RedMap is a pair of proteins derived from the *Arabidopsis thaliana* plant phytochrome that uses phycocyanobilin (PCB) as a cofactor to dimerize PhyA (a naturally occurring red/far-red light-responsive photoreceptor) and FHY1 (a shuttle protein that sequesters PhyA to the nucleus) (25). In contrast, MagRed (45) and NanoReD (21) are dimerization systems derived from the bacterial phytochrome in *Deinococcus radiodurans*, which requires biliverdin, an endogenous cofactor available in mammalian cells. While MagRed includes a full-length DrBphP (a naturally occurring bacterial phytochrome) and Aff6 affibody (de novo engineered binder), NanoReD consists of a truncated DrBphP (histidine kinase removed) and an LDB3 nanobody (de novo engineered binder).

We conducted the dimerization screen in human embryonic kidney (HEK) cells to identify the highest performing LIDs. We transfected two split halves of a recombinase fused to dimerization domains in addition to a green fluorescent protein (GFP) reporter and a transfection marker. Split sites were chosen on the basis of previous evidence of inducibility in other chemical-inducible recombinases (22). In the presence of red light (46) (using the optoplate shown in fig. S1), inducible recombinases reconstitute to excise a transcriptional terminator, and this results in GFP expression (Fig. 1A). All split Cre pairs in Fig. 1B have the photoreceptor fused to the C terminus [denoted as PhyA-Cre<sub>[Split Site]-C</sub> for RedMap] and the binder protein fused to the N-terminal fragment of Cre [denoted as Cre<sub>N-[Split Site]</sub>-FHY1 for RedMap].

In this screen, Cre fused to RedMap yielded the greatest number of inducible recombinases. In contrast, Cre fused to MagRed produced one inducible split with high leakiness, and Cre fused to NanoReD showed no inducible activity (Fig. 1B). Within the RedMap-inducible Cre splits, four of the five split sites resulted in increases exceeding 15-fold. Notably, Cre<sub>N229</sub>-FHY1/PhyA-Cre<sub>230C</sub> and Cre<sub>N251</sub>-FHY1/PhyA-Cre<sub>252C</sub> resulted in 33-fold change. Cre<sub>N105</sub>-Aff6/DrBphP-Cre<sub>106C</sub> also dimerized in the presence of red light with a fold change of 5, but leakiness was high, so we selected the RedMap domains for constructing our larger recombinase library (fig. S2). To test whether there was an orientation preference for each dimerization system, we also fused

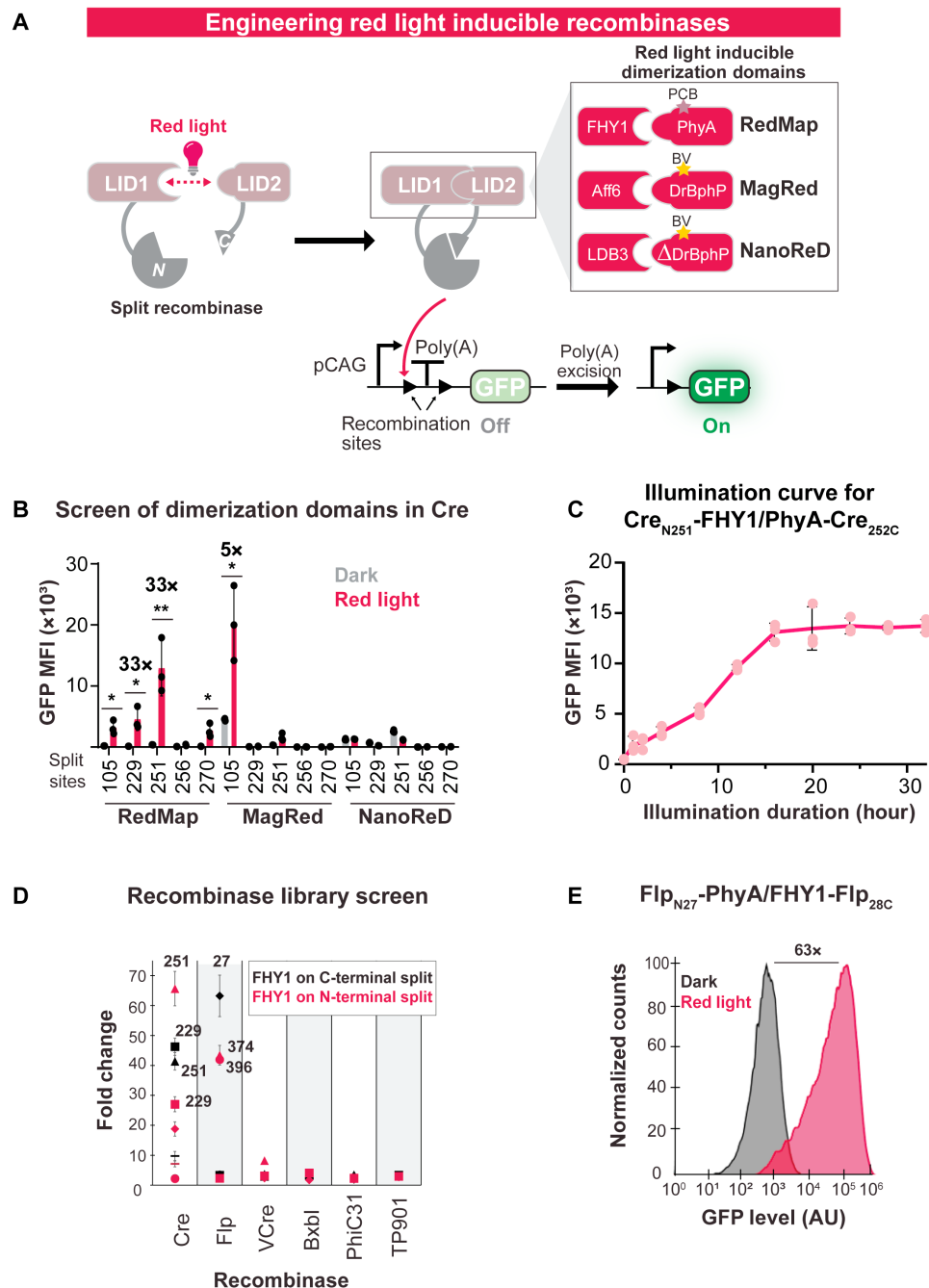


**Fig. 1. Split site screening to develop a library of high-performing red light-inducible recombinases in mammalian cells.** (A) Schematic of red light-inducible recombinase circuit. Under red light, recombinase reconstitutes and excises a transcriptional terminator, resulting in a GFP signal. The three red light dimerization domains tested are RedMap, MagRed, and NanoReD with corresponding cofactor indicated by star. (B) Screen of dimerization domains in five Cre split sites in HEK cells. Split Cre<sub>N229</sub>-FHY1/PhyA-Cre<sub>230C</sub> and Cre<sub>N251</sub>-FHY1/PhyA-Cre<sub>252C</sub> show the highest fold changes of 33X. x axis denotes the final residue of the N-terminal fragment. *P* values were calculated by two-tailed unpaired *t* test and from left to right: *P* = 0.0108, *P* = 0.0146, *P* = 0.0086, *P* = 0.0161, and *P* = 0.0114. (C) Illumination curve indicates optimal light exposure is 20 hours at 0.2 mW/cm<sup>2</sup>. (D) Results of screen fusing RedMap domains to split Cre, Flp, VCre, Bxb1, PhiC31, and TP901. Transfection marker gated for top 50% of cells to screen activity of highly expressed split recombinases in HEK cells. (E) Histograms of GFP expression under dark or illuminated conditions for Flp<sub>N27</sub>-PhyA/FHY1-Flp<sub>28C</sub> show a 63-fold increase. Fold changes were calculated as the ratio of reporter activity with illuminated recombinases over reporter activity with recombinases in the dark. Red light was illuminated at 0.2 mW/cm<sup>2</sup>. Data represented as mean values ± SD (*n* = 3). All source data are provided in the source data file.

each domain to the other split Cre piece (fig. S3). Similar to the first orientation screened, Cre fused to RedMap showed the highest fold changes of inducibility from light to dark.

We optimized reporter activation of Cre fused to RedMap through transfection of Cre<sub>N251</sub>-FHY1/PhyA-Cre<sub>252C</sub> in HEK cells. To increase the GFP signal, we illuminated transfected HEK cells at 660 nm from 1 to 32 hours at 0.2 mW/cm<sup>2</sup>, and the highest fold change in reporter expression occurred at 20 hours (Fig. 1C). We additionally titrated intensity and pulse duration of red light for 20 hours (fig. S4A) and intensity for 1 hour (fig. S4B). We also conducted a PCB dose curve that revealed that 100  $\mu$ M PCB enabled the highest fold change in reporter expression (fig. S5).

After conducting a screen of LIDs with split Cre, we also fused RedMap domains to split Flp, VCre, BxbI, PhiC31, and TP901 recombinases (Fig. 1D). We hypothesized that split sites, which exhibited strong inducibility when fused to chemical-inducible domains (CIDs), would likewise be effective with LIDs. Ten red light-inducible recombinases exhibited a fold change over 8 [raw mean fluorescence intensity (MFI) values are shown in fig. S6, A to G]. The top-performing Flp recombinase was Flp<sub>N27</sub>-PhyA/FHY1-Flp<sub>28C</sub>, which showed a fold change of 63 (Fig. 1E). We also conducted a head-to-head comparison of our top performing red light-inducible Flp with a previously published split Cre using MagRed (38). In our hands, Flp<sub>N27</sub>-PhyA/FHY1-Flp<sub>28C</sub> had a fold change of 42. Meanwhile, Cre<sub>N104</sub>-Aff6/DrBphP-Cre<sub>106C</sub> had a fold change of 4.5 (fig. S7). In our screen of RedMap fused to split recombinases, there was little orientation preference for inducible split sites. Six inducible splits had the FHY1 domain on the N terminus, while four had the FHY1 domain on the C terminus (fig. S8A). We additionally quantified the percentage of split sites that remained inducible when the previously studied CIDs were changed to RedMap domains. A total of 60% of the Cre inducible split sites remained inducible after being fused to RedMap domains instead of CIDs, but this percentage dropped to 37.5% for Flp and 16.66% for VCre (fig. S8B).

### Red light-inducible myogenesis switch in C3H10T1/2 cells

An optogenetic recombinase would be particularly useful in cell fate patterning. We leveraged red light-inducible recombinases in C3H10T1/2 mouse fibroblast cells, which are commonly used to study cell fate decisions (47, 48). C3H10T1/2 cells can differentiate into myotubes through overexpression of the master transcription factor MyoD (49–51). Upon MyoD induction by red light, our engineered C3H10T1/2 cells are expected to form myotubes, which are multinucleated, elongated cells (Fig. 2A).

We initially designed a nonamplifying MyoD circuit, in which we transduced VP64-MyoD in a Flp-Excision (FLEX) switch and transfected Flp recombinase into C3H10T1/2 cells (C3H<sub>myod</sub>) (fig. S9A) (52). After illuminating C3H<sub>myod</sub> cells for 12 hours, we observed morphological changes under the microscope for transfected wild-type (WT) Flp but not for transfected Flp<sub>N396</sub>-FHY1/PhyA-Flp<sub>397C</sub>. Previous studies have calculated changes in myotube formation with Western blots (53) and reverse transcription quantitative polymerase chain reaction of MyoD (50), as well as mean myosin heavy chain (MHC) pixel intensity and MHC area with overlapping 4',6-diamidino-2-phenylindole (DAPI)-stained nuclei (51, 54). We sought to quantify cell fate change using a method that would also capture the morphological changes to these cells. To quantify cell fate changes, we developed a semi-automated image processing algorithm to quantify myotube number by identifying cells stained for anti-MHC conjugated to Alexa Fluor 488 with more than one

nucleus. Our algorithm classifies structures as a myotube within the MHC channel if there are at least two overlapping nuclei (fig. S10). Thus, to confirm myotube formation, we immunostained C3H<sub>myod</sub> cells with anti-MHC and DAPI, and we quantified 157 myotubes formed with WT Flp and 0 with Flp<sub>N396</sub>-FHY1/PhyA-Flp<sub>397C</sub> (fig. S9, B and C).

Next, we engineered an amplification layer to increase the expression of VP64-MyoD after red light reconstitution of split Flp (fig. S9D). In the presence of red light, transfected split Flp will excise mCherry and turn on a reverse tetracycline-regulated transactivator (rtTA). Then, rtTA will bind upstream of a Tre promoter to activate the expression of VP64-MyoD. We transduced the rtTA FLEX switch and MyoD plasmid into C3H10T1/2 cells (C3H<sub>rtTA</sub>) and then transfected Flp<sub>N396</sub>-FHY1/PhyA-Flp<sub>397C</sub>. Following 12 hours of red light exposure, we counted an average of 90 myotubes compared to 8 identified in the dark condition, most likely due to spontaneous reconstitution of recombinases at high concentrations (fig. S9, E to I). We also calculated the mean MHC pixel intensity for C3H<sub>rtTA</sub> cells in the dark or red light illuminated, showing an increase in MHC under red light (fig. S11).

To further improve our circuit and remove the necessity of doxycycline induction, we replaced rtTA with tetracycline-controlled transactivator (tTA) in the amplification layer (Fig. 2A). We also transduced Flp<sub>N396</sub>-FHY1/PhyA-Flp<sub>397C</sub> in addition to the amplification circuit into C3H10T1/2 cells (C3H<sub>tTA</sub>). Using this method, we illuminated C3H<sub>tTA</sub> cells with increasing red light energy doses and saw a corresponding increase in the number of myotubes (fig. S12). Furthermore, we were able to induce myogenesis with spatio-temporal control using just 30 min (63 mJ) of red light, but 1.5 hours of red light illumination showed the best patterning (Fig. 2, B and C). We calculated 55 myotubes on the illuminated side and 5 on the dark side (Fig. 2D and figs. S13 and S14). In addition, we calculated 305 fused cells under illumination and 24 in the dark, which is quantified as the overall number of nuclei within all of the identified myotubes (Fig. 2E). Last, we showed the distribution of myotube area and nuclei number of Fig. 2B to showcase the variety of myotube structures observed under illumination (Fig. 2, F and G).

### Multichromatic Boolean logic

Next, we shifted our focus from exclusively using red light-inducible recombinases to multiplexing red and blue light-inducible recombinases. We conducted a pairwise screen in HEK cells by combining our best performing blue light-inducible recombinases (22) with red light-inducible recombinases from Fig. 1D. First, we tested the orthogonality of the RedMap and Magnet dimerization systems and showed that Flp<sub>N396</sub>-FHY1/PhyA-Flp<sub>397C</sub> only responded to red light (fig. S15A). Similarly, Cre<sub>N251</sub>-nMag/pMag-Cre<sub>252C</sub> only responded to blue light (fig. S15B). After confirming the orthogonality of our LIDs, we used an AND gate reporter to efficiently identify Cre and Flp pairs that simultaneously activated when illuminated (Fig. 3A).

We tested all possible pairwise combinations of Cre and Flp. We found that the combination of red light-inducible Flp with blue light-inducible Cre yielded six inducible pairs (Fig. 3B); meanwhile, red and blue light alone were insufficient to activate the reporter (Fig. 3C). In comparison, blue light-inducible Flp combined with red light-inducible Cre showed no inducible hits (fig. S16). Following this AND gate screen, we proceeded to test the high-performing pairs with our laboratory's BLADE two-input decoder.

BLADE is a modular recombinase circuit architecture that takes in Cre and Flp as inputs (Fig. 3D). In circuits with a single reporter



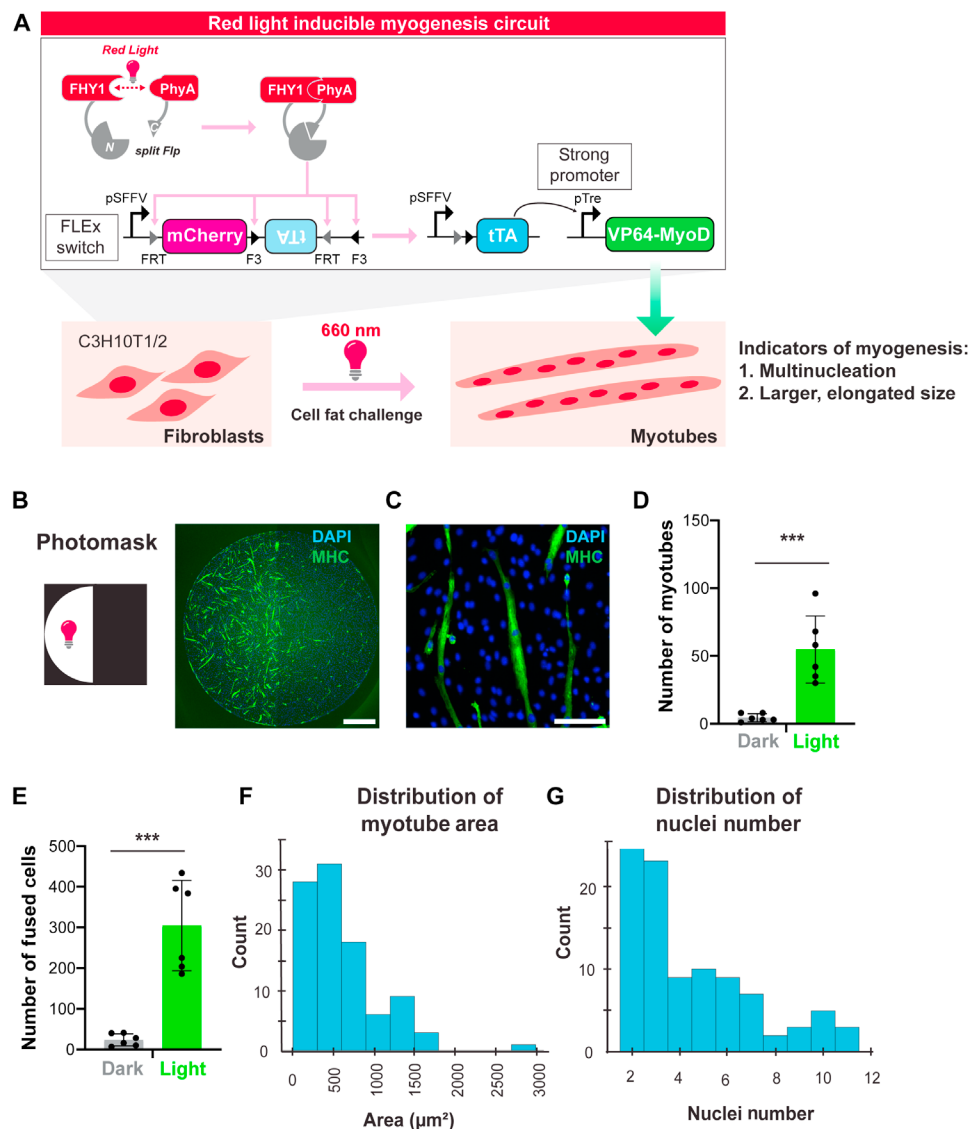


**Fig. 2. Patterned red light-inducible myogenesis switch in C3H10T1/2 cells.** (A) Illustration of myogenesis circuit transduced into C3H10T1/2 cells. Transduced Flp reconstitutes under red light illumination and inverts the sequence encoding tTA. tTA then binds upstream of VP64-MyoD to induce myogenesis. Engineered C3H10T1/2 mouse fibroblasts differentiate into myotubes upon red light illumination due to increased MyoD expression. (B) C3H10T1/2 cells transduced with tTA FLEX switch, inducible MyoD, and Flp<sub>N396</sub>-FHY1/PhyA-Flp<sub>397C</sub> (denoted as C3H<sub>tTA</sub> cells). Representative image after illumination through a photomask. Nuclei were stained with DAPI (blue) and myotubes with anti-MHC (green). Scale bar, 1 mm. (C) Higher magnification image of C3H<sub>tTA</sub> cells. Scale bar, 0.25 mm. (D) Overall number of myotubes counted for C3H<sub>tTA</sub> cells on the left (illuminated) versus right (dark) side of photomask illuminated wells. *P* value was calculated as a two-tailed unpaired *t* test, *P* = 0.0006. Data represented as mean values  $\pm$  SD (*n* = 6). (E) Overall number of fused cells counted for C3H<sub>tTA</sub> cells on the left (illuminated) versus right (dark) side of the well. *P* value was calculated as a two-tailed unpaired *t* test, *P* = 0.0001. Data represented as mean values  $\pm$  SD (*n* = 6). (F) Histogram showing the distribution of myotube area ( $\mu\text{m}^2$ ). (G) Histogram showing the distribution of the number of nuclei. Cells were illuminated with red light for 1.5 hours at 0.5 mW/cm<sup>2</sup>. All source data are provided in the source data file.

per recombinase, recombinases have control over one gene cassette each, but while using BLADE, there is access to an additional, unique third output when both recombinases reconstitute. BLADE was transfected in HEK cells along with Flp<sub>N396</sub>-FHY1/PhyA-Flp<sub>397C</sub> and Cre<sub>N251</sub>-nMag/pMag-Cre<sub>252C</sub> (Fig. 3D). We observed that the expected patterns of the reporter were expressed in accordance with the Boolean logic (Fig. 3D and fig. S17). In the dark, there was no fluorescent protein expression because no active recombinases were reconstituted. In the presence of blue light, split Cre reconstituted, which turned on GFP expression. Similarly, in the presence of red light, split Flp was

reconstituted and switched on near-infrared fluorescent protein (iRFP) expression. Last, in the presence of both wavelengths, mRuby was expressed. GFP and iRFP basal expression occurred under dual red and blue light illumination because Cre and Flp excised DNA unevenly.

### Single and dual wavelength spatial patterning

To explore spatiotemporal control using these tools, we patterned gene outputs in HEK cells using a single red wavelength and dual wavelengths of red and blue light. Initially, we focused on red light patterning

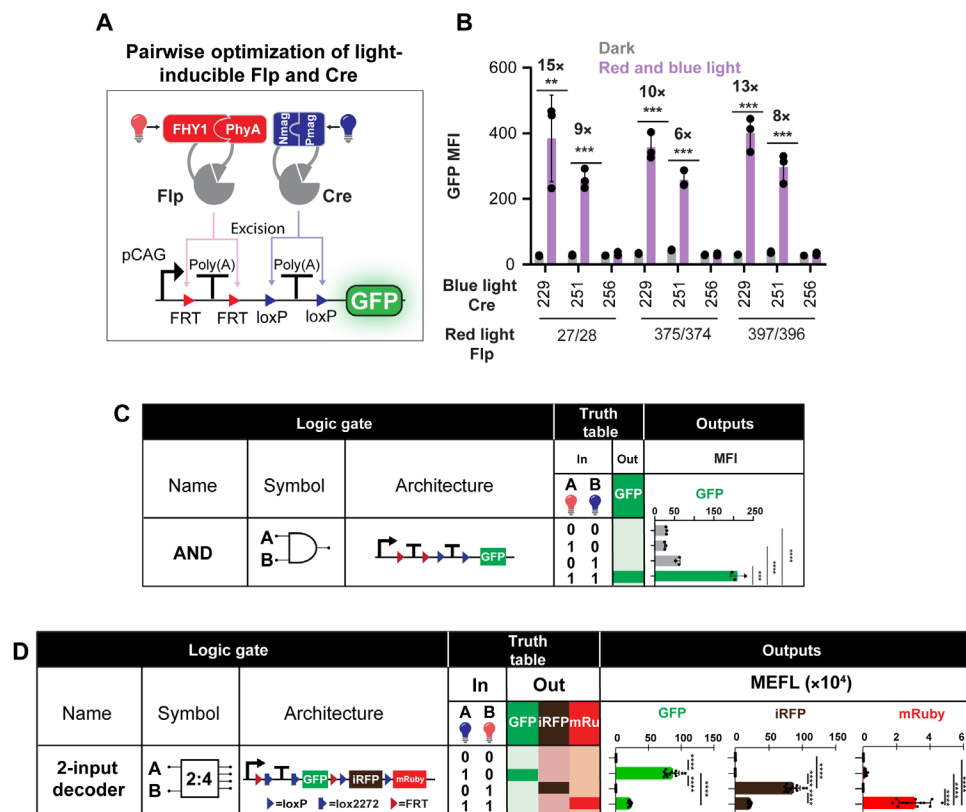


**Fig. 3. Multiplexing red and blue light-inducible recombinases.** (A) Schematic of red and blue light-inducible Cre and Flp circuit transfected into HEK cells. GFP is designed to express only in the presence of both wavelengths. (B) Multiplexed red light-inducible Flp with blue light-inducible Cre. Fold changes were calculated as the ratio of reporter activity with illuminated recombinases over reporter activity with recombinases in the dark. *x* axis denotes the final residue of the N-terminal fragment. *P* values were calculated as two-tailed unpaired *t* tests and from left to right: *P* = 0.0093, *P* = 0.0002, *P* = 0.0002, *P* = 0.0001, *P* = 0.0002, and *P* = 0.0005. Data represented as mean values  $\pm$  SD (*n* = 3). (C) Flp<sub>N396</sub>-FHY1/PhyA-Flp<sub>397C</sub> and Cre<sub>N251</sub>-nMag/pMag-Cre<sub>252C</sub> transfected with the AND gate and either illuminated with red light, blue light, both red and blue light, or no light. *P* values were calculated as two-tailed unpaired *t* tests. \*\**P* < 0.01, \*\*\**P* < 0.001, and \*\*\*\**P* < 0.0001. (D) Schematic of BLADE two-input, four-output decoder transfected in HEK cells. Cre excises lox sites (blue arrows) to express GFP, Flp excises FRT sites (red arrows) to express iRFP, and the presence of both recombinases is designed to express mRuby. Table of light inputs and gene outputs for BLADE transfected with Flp<sub>N396</sub>-FHY1/PhyA-Flp<sub>397C</sub> and Cre<sub>N251</sub>-nMag/pMag-Cre<sub>252C</sub>. Red light was pulsed for 5 min on and 25 min off for 44 hours at 0.35 mW/cm<sup>2</sup>. Blue light was illuminated 1 day after transfection and was pulsed for 5 min on and 25 min off for 20 hours at 2.5 mW/cm<sup>2</sup>. Transfection marker gated for top 40% of cells to screen activity of highly expressed split recombinases in HEK cells. *P* values were calculated as two-tailed unpaired *t* test where for \*\*\*\**P* < 0.0001. Data represented as mean equivalent fluorochrome values  $\pm$  SD (*n* = 12). All source data are provided in the source data file. Poly(A), polyadenylate.

and transfected Flp<sub>N396</sub>-FHY1/PhyA-Flp<sub>397C</sub> with a GFP reporter into HEK cells. Then, we illuminated cells through a photomask, and we saw considerable GFP activity in the dark regions. We hypothesized (i) that red light scattered to the off region to reconstitute split Flp and (ii) that basal reconstitution of split recombinases was too high under a CAG promoter. To reduce red light scattering, we plated transfected cells in media containing 0.5 mM brilliant blue, a Food and Drug Administration-approved dye that absorbs light in the 660-nm range (55). The addition of brilliant blue decreased dark activation in patterned wells by 69% (fig. S18). We additionally cloned our split recombinases under a doxycycline-inducible promoter to more easily control Flp expression levels (fig. S19). We saw that doxycycline (2  $\mu$ g/ml) resulted in the greatest fold change for patterning. After implementing the brilliant blue photoabsorber and doxycycline-inducible split Flp, followed by red light illumination, we quantified a steep increase in GFP expression at the photomask boundary (fig. S20).

Next, we transfected Flp<sub>N396</sub>-FHY1/PhyA-Flp<sub>397C</sub> and Cre<sub>N229</sub>-nMag/pMag-Cre<sub>230C</sub> (top performing blue light-inducible Cre) with orthogonal GFP and blue fluorescent protein (BFP) reporters (Fig. 4A).

To pattern half a well with each recombinase reporter, we designed two photomasks which were sequentially attached to the bottom of the plate covering either the right half or top half of each well and then illuminated through the photomask. With this recombinase pair, we conducted a doxycycline curve from which we chose to induce with 0.02  $\mu$ g/ml due to its lower dark activity while preserving high fold change (fig. S21). Then, in Fig. 4 (B and C), we repeated this transfection and after illumination, we observed GFP activated by red light-inducible Flp expressed on the left side, and BFP activated by blue light-inducible Cre was expressed on the right side (fig. S22). Last, we transfected Flp<sub>N396</sub>-FHY1/PhyA-Flp<sub>397C</sub> and Cre<sub>N229</sub>-nMag/pMag-Cre<sub>230C</sub> with an AND gate reporter to see if we could pattern encoded logic (Fig. 4D). We observed substantial GFP activation by the illumination of red and blue light (Fig. 4, E and F, and fig. S23).

### DISCUSSION

Here, we tested three different LIDs with split Cre recombinase and found the highest inducibility with RedMap domains. One drawback

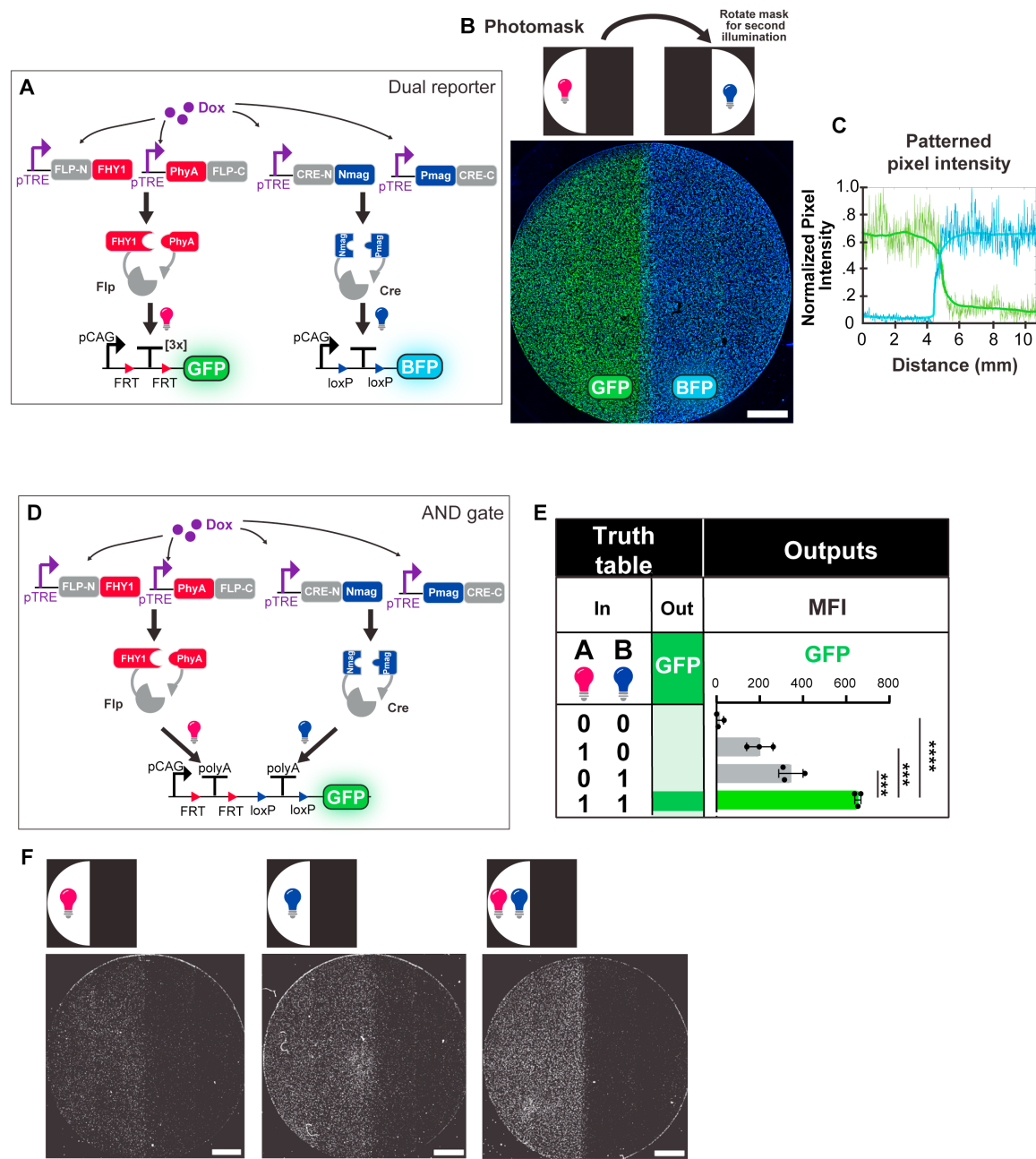


**Fig. 4. Single and dual wavelength spatial patterning.** (A) Diagram of red light-inducible Flp and blue light-inducible Cre circuits transfected for patterning experiments. (B) Image of photomask patterned HEK cells transfected with Flp<sub>N396</sub>-FHY1/PhyA-Flp<sub>397C</sub> and Cre<sub>N229</sub>-pMag/nMag-Cre<sub>230C</sub>. Red light-inducible Flp drives GFP on the left half of the well and blue light-inducible Cre drives BFP expression on the right half of the well. Cells were illuminated with red light at 0.5 mW/cm<sup>2</sup> for 3 min and blue light at 3.5 mW/cm<sup>2</sup> for 5 min. (C) Plot of patterned pixel intensity of red light-inducible Flp and blue light-inducible Cre. In blue is the intensity values for Cre, and green indicates intensity values for Flp. (D) Diagram of red light-inducible Flp and blue light-inducible Cre circuits transfected with AND gate reporter. (E) Table of light inputs and gene outputs for AND gate transfected with Flp<sub>N396</sub>-FHY1/PhyA-Flp<sub>397C</sub> and Cre<sub>N229</sub>-pMag/nMag-Cre<sub>230C</sub>. Cells were illuminated with red and blue light at 0.5 and 3.5 mW/cm<sup>2</sup> for 10 min. (F) Images of photomask patterned HEK cells transfected with Flp<sub>N396</sub>-FHY1/PhyA-Flp<sub>397C</sub>, Cre<sub>N229</sub>-pMag/nMag-Cre<sub>230C</sub>, and an AND gate reporter. Scale bars, 2 mm. All source data are provided in the source data file. \*\*\**P* < 0.001 and \*\*\*\**P* < 0.0001.

of RedMap domains is that the photoreceptor PhyA requires the exogenous addition of PCB compared to MagRed and NanoReD, which do not. Despite this hurdle, in vivo experiments have been done with RedMap-inducible circuits to modulate insulin levels (25). In addition, PCB can be genetically encoded to overcome its delivery challenges (56).

Furthermore, after conducting a screen of RedMap fused to published chemical-inducible recombinases, we were surprised that only 25% of the split sites we tested were inducible. We hypothesized that Cre yielded the most inducible split sites because it has previously performed the most robustly. Our laboratory's best performing chemical-inducible Cre and Flp resulted in a fold change of

around 275 and 418, while the top performing chemical-inducible TP901 and Bxb1 recombinases resulted in a lower fold change around 76 and 32 (22). We are not sure why our split recombinases have lower performance when fused to RedMap domains. We hypothesize that the larger gene sequence of PhyA (around 1.85 kilobase pairs) may lower protein expression relative to smaller dimerization domains (57, 58). In addition, PhyA is a light labile protein, which could reduce the expression of the split protein compared to chemical-inducible proteins.

One shortcoming of this screen was that our high performing split FLP was not strong enough to induce myogenesis in C3H10T1/2 cells without adding an amplification layer. Developing higher performing red light-inducible recombinases in the future could omit the need for this layer of regulation. In addition, after testing nine pairs of red light-inducible Cre and blue light-inducible FLP, none showed ON activity with the AND gate reporter. This was most likely due to the lower performance of the blue light-inducible FLP recombinases compared to the blue light-inducible Cre recombinases (22). Last, our AND gate circuit performance could be further optimized to reduce red and blue light activation of the GFP reporter. These results highlight the importance of developing a collection of high performing recombinases with a large fold change. Our current method uses manual cloning of all subsets of split recombinases. However, exploring all possible splits is not tractable. In the future, it would be beneficial to complement empirical testing with protein structural prediction tools such as AlphaFold while developing a collection of split proteins. Furthermore, the directed evolution of RedMap domains could improve activation kinetics for future applications.

While we and others have demonstrated the utility of individual light-inducible recombinases, here we multiplex red and blue light-inducible recombinases in mammalian cells. This toolset expands the type of gene regulation possible to encompass Boolean logic not possible with just one wavelength. Future optogenetic recombinase collections should focus on increasing the number of orthogonal light-inducible tools to increase the complexity of Boolean logic that can be done. Traditionally, optogenetic SSRs have been leveraged for targeted integration or excision of DNA in the development of transgenic animals and in vitro tissue models (59, 60). We envision the light-inducible genetic reprogramming of cells will enable mechanistic investigations of cell biology and the development of multicellular engineering living systems. For example, it is well documented that overexpression of transcription factors can direct cell differentiation (50, 61). In the future, the fluorescent proteins in our BLADE circuit could be swapped for transcription factors and then integrated into induced pluripotent stem cells (iPSCs) to spatially control cell fate. Sustained gene expression is often needed in various disease and cell fate pathway modeling (62, 63). While existing multichromatic circuits require continuous illumination for persistent perturbation, permanently encoded outputs to minimize illumination could reduce toxicity. Conversely, we also recognize that transient methods of gene induction are more likely to reach a lower equilibrium of basal activity compared to recombinases, which have irreversible dark activity that may compound over time.

While optogenetics uniquely uses light to control protein activity and downstream gene expression, complementary fields such as biomaterials (64) and three-dimensional (3D) bioprinting (65) also strive to control cell signaling and geometry through controlled depots and precise cell deposition. These fields have achieved great advancements

in spatial control, but biomaterials and 3D printing alone cannot introduce engineered signaling circuits with sustained signals and genetically encoded logic. Sustained signals are present in a multitude of endogenous cellular pathways, such as control over cell fate (34, 35). Meanwhile, genetically encoded logic increases the number of controllable orthogonal outputs and the complexity of circuits we can design. Multichromatic gene schemes hold the potential to demonstrate sustained signals and genetically encoded logic, although existing publications do not exhibit this. Overall, optogenetics holds tremendous promise in its ability to spatiotemporally control regulatory proteins. This will solve a fundamental problem in regenerative medicine in solving how to orchestrate spatial activation and repression of gene expression within native tissues.

The promise of optogenetics lies in the power to spatially control outputs. Thus, it is crucial to demonstrate spatial control and to design more complex spatial patterns with the help of logic to push the number of gene perturbations possible with optogenetics. We anticipate that the tools developed in this work will expand the circuit-encoded logic possible within mammalian cells for pivotal advances in genetically engineering more spatiotemporally precise cellular patterning.

## MATERIALS AND METHODS

### Mammalian cell culture

HEK293FT and C3H10T1/2 cells were cultured at 37°C with 5% CO<sub>2</sub>. HEK cells were maintained in Dulbecco's modified Eagle's medium containing 5% fetal bovine serum, 1% penicillin and streptomycin (Corning 3000IC1), 1% L-glutamine (Corning 2500SCI), and 1% sodium pyruvate (Lonza, 13115E). C3H10T1/2 cells were maintained in Eagle's minimum essential medium supplemented with 10% fetal bovine serum, 2 mM L-glutamine, and penicillin (50 UI/ml) and streptomycin. C3H10T1/2 cells were not maintained above passage 15.

### Inducible split recombinase and reporter plasmid construction

RedMap domains (25) FHY1 and PhyA were ordered as g-block sequences (Invitrogen) with homologous stretches that overlapped with the Cre backbone for Gibson assembly. The MagRed domains (45) were also ordered as gBlocks (Invitrogen), and the NanoReD domains (21) were a gift from L. Gu. All other plasmids were cloned using restriction enzyme digestion and Gibson assembly. All constructs confirmed via a test cut run on gel electrophoresis and then sent for sanger sequencing from Quintara Biosciences. Construct information in table S1.

### Small-molecule preparation

PCB (SiChem, SC-1800) was dissolved in 100% dimethyl sulfoxide to a final 100 mM stock and stored at −20°C. Doxycycline (Gold Biotechnology, D-500-1) was dissolved in water to a final concentration of 2 µg/ml and stored at −20°C.

### Optoplate calibration

To calibrate each optoplate, we used optoConfig-96 software (66) to program 14 increasing intensity values between 0 and 4000. For each wavelength, we measured triplicate power reads using a USB power meter (Thorlabs, PM16-120). Then, we made a standard curve to calculate the intensity value of each grayscale intensity input on the optoConfig-96.



### HEK transfection, illumination, and flow cytometry

For flow cytometry experiments, HEK293FT cells were plated in triplicate at 20,000 cells per well in a black-walled 96-well plate and then transfected the next day at 70 to 80% confluency. In each split red light–recombinase screen, cells were transfected using polyethylenimine (0.323 g/liter; PEI) (Polysciences, 23966-2) dissolved in 0.15 M NaCl (4 parts PEI:25 parts NaCl). After a 10-min incubation of DNA added to the PEI–NaCl complex, 10- $\mu$ l transfection volume was dispensed per well. Transfection ratios for red light–inducible screens are detailed in table S2. Two hours after transfection, PCB was added to cells at a final concentration of 100  $\mu$ M. Twenty-four hours after transfection, cells were illuminated for 20 hours at 0.2 mW/cm<sup>2</sup> using an optoplate (46), which was programmed using optoConfig 96 software (fig. S1) (66). Forty-eight hours after transfection, HEK cells were analyzed using a Thermo Fisher Attune Nxt cytometer.

Transfection for the multiplexing screen with AND gate reporter was conducted in triplicate according to ratios detailed in table S3. BLADE experiments were transfected in six replicates according to DNA ratios in table S4. Then, two wells were pooled together for flow cytometry analysis. Both the AND gate and BLADE transfections were induced with PCB 2 hours post-transfection. Then, 2 hours after drug induction, illumination for the AND gate and BLADE experiments was initiated. For both Boolean logic gates, red light was pulsed for 5 min on and 25 min off for 44 hours at 0.35 mW/cm<sup>2</sup>. Blue light was illuminated 1 day after transfection and was pulsed for 5 min on and 25 min off for 20 hours at 2.5 mW/cm<sup>2</sup>. BLADE transfection fluorescence channel measurements were converted to molecules of equivalent fluorescein units using SPHERO calibration beads (Spherotech, RCP-30-5A).

### HEK transfection, illumination, and microscopy

HEK293FT cells were seeded into a T-75 at 4.8 million cells per flask. The following day, HEK cells were transfected at around 70 to 80% confluency with 19,500 ng in total of circuit components and then wrapped in aluminum foil. Transfection ratios are detailed in tables S5 to S7. The next day, the cells were passaged in the dark and reseeded into a black-walled 24-well plate (Ibidi, 82406) at 1 million cells per well. For red light patterning, cells were seeded in media with 0.22- $\mu$ m filtered 0.5 mM brilliant blue (Spectrum, FD110-100GM), 100  $\mu$ M PCB, and doxycycline (2  $\mu$ g/ml). For red and blue light patterning, cells were seeded in media with 0.22- $\mu$ m filtered, 0.5 mM brilliant blue and 2 mM tartrazine (Chem-Impex, 22937), 100  $\mu$ M PCB, and doxycycline (0.02  $\mu$ g/ml). Five hours later, cells were illuminated with an Acetal (McMaster-Carr, 8492 K212)–based photomask taped underneath the culture plate. A 0.125-inch Acetal was laser cut with Epilog Engraver using a speed of 30 and a power of 100 in raster mode and then a speed of 30 and maximum power and frequency in vector mode. Illumination for patterning was done with an Red, Green, Blue (RGB) projector (EKB Technologies, DPM-E4500MKIIRGBHPCR-OX). Red light illumination was 3 min at 0.5 mW/cm<sup>2</sup>. For red and blue light illumination with individual recombinase reporters, red light illumination was the same as single red wavelength patterning, and blue light illumination was 5 min at 3.5 mW/cm<sup>2</sup>. The AND gate was illuminated for 10 minutes, with red light set at 0.5 mW/cm<sup>2</sup> and blue light at 3.5 mW/cm<sup>2</sup>. Cell imaging was done the next day on a BioTek Cytation 5 imaging reader. Pixel intensity was measured over each well in Fiji. Raw pixel intensity values were smoothed using the moving average function in MATLAB.

### C3H10T1/2 transfection

C3H10T1/2 cells were plated at 5000 cells per well in a black-walled 96-well plate and transfected the following day with Lipofectamine 3000 according to the manufacturer's protocol (100 DNA ng per well).

### Lentivirus production for C3H10T1/2 cells

HEK cells were initially plated at 4.8 million cells in a T-75. The next day, at around 80% confluency, HEK cells were transfected with 9.43  $\mu$ g of viral packaging DNA (6.43  $\mu$ g of pDelta, 2.14  $\mu$ g of pVsvg, and 0.86  $\mu$ g of pAdv) and 2.1  $\mu$ g of plasmid of interest (concentrated at more than 1  $\mu$ g/ $\mu$ l) with 0.16 fraction PEI in 0.15 M NaCl. Media was changed the following day, and for the next 2 days, the virus was collected and stored at 4°C. On day 5, the virus was spun down at 1200g for 10 min at 4°C to remove cellular debris. The supernatant was then transferred to a new conical and concentrated with centrifugal filters (EMD Millipore, UFC801024).

### C3H10T1/2 cell transduction and myogenesis experiment

C3H10T1/2 cells were plated at 100,000 cells per well in 2.5 ml in a six-well plate. The next day, all virus was added dropwise to C3H10T1/2 cells along with 1  $\mu$ l of polybrene (10 mg/ml; EMD Millipore, TR-1003-G). C3H<sub>myoD</sub> cells were transduced with MyoD nonamplifying circuit. C3H<sub>rtTA</sub> cells were transduced with rtTA FLEX switch and MyoD plasmid in a 1:1 ratio. C3H<sub>tTA</sub> cells were transduced with tTA FLEX switch, MyoD plasmid, and Flp<sub>N396</sub>-FHY1/PhyA-Flp<sub>397C</sub> in a 1:1:1 ratio. Cells were passaged for the next 2 days, and on the second day, cell transduction efficiency was confirmed via flow cytometry. Transduced C3H10T1/2 cells were plated in a black-walled 96-well plate at 5000 cells per well, and then C3H<sub>myoD</sub> and C3H<sub>rtTA</sub> cells were transfected with Flp<sub>N396</sub>-FHY1/PhyA-Flp<sub>397C</sub> the following day with Lipofectamine 3000. Two hours post-transfection, cells were induced with 100  $\mu$ M PCB. C3H<sub>rtTA</sub> cells were also induced with doxycycline (a final concentration of 2  $\mu$ g/ml). Cells were illuminated at 660 nm the next day for 12 hours at 0.2 mW/cm<sup>2</sup> using our optoplate for C3H<sub>myoD</sub> and C3H<sub>rtTA</sub> cells. C3H<sub>tTA</sub> cells were illuminated for 1.5 hours at 0.5 mW/cm<sup>2</sup> using our projector. In fig. S12, we expressed the illumination conditions as an energy dose (mJ), the product of the power density (mW/cm<sup>2</sup>), and the exposure duration (s). The day following illumination, cell medium was changed, and C3H<sub>tTA</sub> cells were fixed 2 days later. For C3H<sub>myoD</sub> and C3H<sub>rtTA</sub> cells, cells were fixed 1 week after transfection, and cell medium was changed every 2 days (doxycycline was added every 2 days for C3H<sub>rtTA</sub> cells).

### C3H10T1/2 cell immunostaining

Cells were initially fixed using 4% paraformaldehyde. After fixation, cells were treated with permeabilization solution [0.5% Triton X-100 in phosphate-buffered saline (PBS)] for 10 min and then blocking solution (1% bovine serum albumin in PBS) for 30 min. Next, cells were stained with anti-MHC conjugated to Alexa Fluor 488 (Developmental Studies Hybridoma Bank, MF-20) and diluted in washing solution (0.01% Triton X-100 in PBS) at 4°C overnight. The next morning, cells were washed twice and then incubated at room temperature with anti-mouse immunoglobulin G Alexa Fluor 488 (Thermo Fisher Scientific, A-21202) diluted in wash solution for 1 hour. Afterward, the cells were washed twice with wash solution and lastly were counterstained with DAPI (1 ng/ml) for 30 min. Last, the cells were washed once with PBS and stored in PBS at 4°C.

## Microscopy

Fluorescence microscopy was performed using the BioTek Cytation 5 Cell Imager. A 4× objective was used to collect images at 37°C, 5% CO<sub>2</sub>, and 90% humidity. For imaging of mCherry, a 554 light-emitting diode (LED) cube was paired with an Ex556/Em600 filter cube. To image GFP and Alexa Fluor 488, a 465 LED cube was paired with an Ex469/Em525 filter cube, and to measure BFP and DAPI, a 365 LED cube was paired with an Ex377/Em447 filter cube.

Confocal microscopy was performed using the Nikon Ti2-E with Andor Dragonfly 505 System. A 20× objective was used to collect images at room temperature. To image anti-MHC conjugated to Alexa Fluor 488, a 465 LED cube was paired with an Ex469/Em525 filter cube, and to measure DAPI, a 365 LED cube was paired with an Ex377/Em447 filter cube.

## Image processing software

We developed a semi-automated script to segment and characterize myotube structures in imaging data, which we implemented in MATLAB. The inputs to the script are fluorescence images of myotubes (i.e., cells stained against MHC) and of nuclei, and the outputs are a series of measurements including a number of myotubes, geometric properties of myotubes, and number of nuclei per myotube. Within the script, the input images are binarized with a user-defined threshold and preprocessed to remove noise. Connected sets of pixels within the MHC channel are classified as candidate myotubes or non-myotubes based on empirically determined thresholds for area and eccentricity. The nuclei channel is used to determine the number of nuclei associated with each candidate myotube, and candidates with a single nucleus are discounted. Because of the complex morphologies of myotubes and the challenges associated with completely automated segmentation, we included an interactive quality control step where the user can manually discount myotubes that were incorrectly identified.

## Flow cytometry

For red light domain and split site screening experiments, HEK cells were passaged and resuspended in HEK media. All samples were gated for viability on a flow cytometer using the forward scatter and side scatter. Then, transfected populations were gated for a transfection marker and subsequently measured for GFP MFI within that population. No fewer than 10,000 cells were looked at for each sample. Fluorescence data were collected for iRFP (excitation laser: 638 nm, emission: 720/30 nm), GFP (excitation laser: 488 nm, emission: 510/10 nm), mCherry/mRuby (excitation laser: 561 nm, emission: 620/15 nm), and LsmOrange (excitation laser: 405 nm, emission: 603/48 nm). Flow cytometry data were then analyzed using FlowJo.

## Statistical methods

All transient experimental analysis via flow cytometry included at least three separate cell culture transfections. Fluorescence intensity values were then averaged, and SD was reported. All statistical analysis was performed within Prism 8.

## Supplementary Materials

### The PDF file includes:

Figs. S1 to S23

Tables S1 to S7

Legends for data S1 to S12

Legend for code S1

### Other Supplementary Material for this manuscript includes the following:

Data S1 to S12

Code S1

## REFERENCES AND NOTES

1. K. Deisseroth, Optogenetics: 10 years of microbial opsins in neuroscience, *Nat. Neurosci.* **18**, 1213–1225 (2015).
2. S. S. Skeeters, T. Camp, H. Fan, K. Zhang, The expanding role of split protein complementation in opsin-free optogenetics, *Curr. Opin. Pharmacol.* **65**, 102236 (2022).
3. L. Petreanu, D. Huber, A. Sobczyk, K. Svoboda, Channelrhodopsin-2-assisted circuit mapping of long-range callosal projections, *Nat. Neurosci.* **10**, 663–668 (2007).
4. H. Wang, J. Peca, M. Matsuzaki, K. Matsuzaki, J. Noguchi, L. Qiu, D. Wang, F. Zhang, E. Boyden, K. Deisseroth, H. Kasai, W. C. Hall, G. Feng, G. J. Augustine, High-speed mapping of synaptic connectivity using photostimulation in Channelrhodopsin-2 transgenic mice, *Proc. Natl. Acad. Sci. U.S.A.* **104**, 8143–8148 (2007).
5. A. R. Adamantidis, F. Zhang, A. M. Aravanis, K. Deisseroth, L. de Lecea, Neural substrates of awakening probed with optogenetic control of hypocretin neurons, *Nature* **450**, 420–424 (2007).
6. O. G. S. Ayling, T. C. Harrison, J. D. Boyd, A. Goroshkov, T. H. Murphy, Automated light-based mapping of motor cortex by photoactivation of channelrhodopsin-2 transgenic mice, *Nat. Methods* **6**, 219–224 (2009).
7. X. Liu, S. Ramirez, P. T. Pang, C. B. Puryear, A. Govindarajan, K. Deisseroth, S. Tonegawa, Optogenetic stimulation of a hippocampal engram activates fear memory recall, *Nature* **484**, 381–385 (2012).
8. M. Siddiqui, C. Tous, W. W. Wong, Small molecule-inducible gene regulatory systems in mammalian cells: Progress and design principles, *Curr. Opin. Biotechnol.* **78**, 102823 (2022).
9. Z. H. Dennis, W. Benman, L. Dong, L. J. Bugaj, Rapid optogenetic clustering in the cytoplasm with BcLOVclust, *J. Mol. Biol.* **436**, 168452 (2024).
10. I. W. Chen, E. Ronzitti, B. R. Lee, T. L. Daigle, D. Dalkara, H. Zeng, V. Emiliani, E. Papagiakoumou, In Vivo submillisecond two-photon optogenetics with temporally focused patterned light, *J. Neurosci.* **39**, 3484–3497 (2019).
11. L. G. M. Heezen, T. Abdelaal, M. van Putten, A. Aartsma-Rus, A. Mahfouz, P. Spitali, Spatial transcriptomics reveal markers of histopathological changes in Duchenne muscular dystrophy mouse models, *Nat. Commun.* **14**, 4909 (2023).
12. W. Chen, C. Li, W. Liang, Y. Li, Z. Zou, Y. Xie, Y. Liao, L. Yu, Q. Lin, M. Huang, Z. Li, X. Zhu, The roles of optogenetics and technology in neurobiology: A review, *Front. Aging Neurosci.* **14**, 867863 (2022).
13. J. G. Bernstein, E. S. Boyden, Optogenetic tools for analyzing the neural circuits of behavior, *Trends Cogn. Sci.* **15**, 592–600 (2011).
14. J. I. Spiltoir, C. L. Tucker, Photodimerization systems for regulating protein–protein interactions with light, *Curr. Opin. Struct. Biol.* **57**, 1–8 (2019).
15. A. Flores-Ibarra, R. N. A. Maia, B. Olasz, J. R. Church, G. Gotthardt, I. Schapiro, J. Heberle, P. Nogly, Light-oxygen-voltage (LOV)-sensing domains: Activation mechanism and optogenetic stimulation, *J. Mol. Biol.* **436**, 168356 (2024).
16. A. Pudasaini, K. K. El-Arab, B. D. Zoltowski, LOV-based optogenetic devices: Light-driven modules to impart photoregulated control of cellular signaling, *Front. Mol. Biosci.* **2**, 18 (2015).
17. G. P. Pathak, J. I. Spiltoir, C. Höglund, L. R. Polstein, S. Heine-Koskinen, C. A. Gersbach, J. Rossi, C. L. Tucker, Bidirectional approaches for optogenetic regulation of gene expression in mammalian cells using Arabidopsis cryptochrome 2, *Nucleic Acids Res.* **45**, e167 (2017).
18. C. N. Hernández-Candia, C. L. Wysoczynski, C. L. Tucker, Advances in optogenetic regulation of gene expression in mammalian cells using cryptochrome 2 (CRY2), *Methods* **164–165**, 81–90 (2019).
19. A. Losi, K. H. Gardner, A. Möglich, Blue-light receptors for optogenetics, *Chem. Rev.* **118**, 10659–10709 (2018).
20. K. Tang, H. M. Beyer, M. D. Zurbriggen, W. Gärtner, The red edge: Bilin-binding photoreceptors as optogenetic tools and fluorescence reporters, *Chem. Rev.* **121**, 14906–14956 (2021).
21. Z. Huang, Z. Li, X. Zhang, S. Kang, R. Dong, L. Sun, X. Fu, D. Vaisar, K. Watanabe, L. Gu, Creating red light-switchable protein dimerization systems as genetically encoded actuators with high specificity, *ACS Synth. Biol.* **9**, 3322–3333 (2020).
22. B. H. Weinberg, J. H. Cho, Y. Agarwal, N. T. H. Pham, L. D. Caraballo, M. Walkosz, C. Ortega, M. Trexler, N. Tague, B. Law, W. K. J. Benman, J. Letendre, J. Beal, W. W. Wong, High-performance chemical- and light-inducible recombinases in mammalian cells and mice, *Nat. Commun.* **10**, 4845 (2019).
23. K. Morikawa, K. Furuhashi, C. de Sena-Tomas, A. L. Garcia-Garcia, R. Bekdash, A. D. Klein, N. Gallerani, H. E. Yamamoto, S. H. E. Park, G. S. Collins, F. Kawano, M. Sato, C. S. Lin, K. L. Targoff, E. Au, M. C. Salling, M. Yazawa, Photoactivatable Cre recombinase 3.0 for in vivo mouse applications, *Nat. Commun.* **11**, 2141 (2020).

24. V. Gligorovski, A. Sadeghi, S. J. Rahi, Multidimensional characterization of inducible promoters and a highly light-sensitive LOV-transcription factor. *Nat. Commun.* **14**, 3810 (2023).
25. Y. Zhou, D. Kong, X. Wang, G. Yu, X. Wu, N. Guan, W. Weber, H. Ye, A small and highly sensitive red/far-red optogenetic switch for applications in mammals. *Nat. Biotechnol.* **40**, 262–272 (2022).
26. L. R. Polstein, C. A. Gersbach, Light-inducible spatiotemporal control of gene activation by customizable zinc finger transcription factors. *J. Am. Chem. Soc.* **134**, 16480–16483 (2012).
27. J. Yu, J. Shin, J. Yu, J. Kim, D. Yu, W. D. Heo, Programmable RNA base editing with photoactivatable CRISPR-Cas13. *Nat. Commun.* **15**, 673 (2024).
28. L. R. Polstein, C. A. Gersbach, A light-inducible CRISPR-Cas9 system for control of endogenous gene activation. *Nat. Chem. Biol.* **11**, 198–200 (2015).
29. K. Muller, R. Engesser, S. Schulz, T. Steinberg, P. Tomakidi, C. C. Weber, R. Ulm, J. Timmer, M. D. Zurbruggen, W. Weber, Multi-chromatic control of mammalian gene expression and signaling. *Nucleic Acids Res.* **41**, e124 (2013).
30. J. Jang, K. Tang, J. Youn, S. McDonald, H. M. Beyer, M. D. Zurbruggen, M. Uppalapati, G. A. Woolley, Engineering of bidirectional, cyanobacteriochrome-based light-inducible dimers (BICYCLs). *Nat. Methods* **20**, 432–441 (2023).
31. M. M. Kramer, W. W. D. Mühlhäuser, W. Weber, G. Radziwill, Multichromatic control of signaling pathways in mammalian cells. *Adv. Biol.* **5**, 2000196 (2021).
32. J. E. Purvis, K. W. Karhohs, C. Mock, E. Batchelor, A. Loewer, G. Lahav, P53 dynamics control cell fate. *Science* **336**, 1440–1444 (2012).
33. T. Holbro, G. Civenni, N. E. Hynes NE, The ErbB receptors and their role in cancer progression. *Exp. Cell Res.* **284**, 99–110 (2003).
34. K. Hirata-Tominaga, T. Nakamura, N. Okumura, S. Kawasaki, E. P. Kay, Y. Barrandon, N. Koizumi, S. Kinoshita, Corneal endothelial cell fate is maintained by LGR5 through the regulation of hedgehog and Wnt pathway. *Stem Cells* **31**, 1396–1407 (2013).
35. L. Vallier, T. Touboul, S. Brown, C. Cho, B. Bilican, M. Alexander, J. Cedervall, S. Chandran, L. Åhrlund-Richter, A. Weber, R. A. Pedersen, Signaling pathways controlling pluripotency and early cell fate decisions of human induced pluripotent stem cells. *Stem Cells* **27**, 2655–2666 (2009).
36. N. D. F. Grindley, K. L. Whiteson, P. A. Rice, Mechanisms of site-specific recombination. *Annu. Rev. Biochem.* **75**, 567–605 (2006).
37. A. L. Garcia-Otin, F. Guillou, Mammalian genome targeting using site-specific recombinases. *Front. Biosci.* **11**, 1108–1136 (2006).
38. Y. Kuwasaki, K. Suzuki, G. Yu, S. Yamamoto, T. Otabe, Y. Kakiyama, M. Nishiwaki, K. Miyake, K. Fushimi, R. Bekdash, Y. Shimizu, R. Narikawa, T. Nakajima, M. Yazawa, M. Sato, A red light-responsive photoswitch for deep tissue optogenetics. *Nat. Biotechnol.* **40**, 1672–1679 (2022).
39. A. C. Hughes, B. G. Pittman, B. Xu, J. W. Gammons, C. M. Webb, H. G. Nolen, P. Chapman, J. B. Bikoff, L. A. Schwarz, A single-vector intersectional AAV strategy for interrogating cellular diversity and brain function. *Nat. Neurosci.* **27**, 1400–1410 (2024).
40. L. E. Fenno, J. Mattis, C. Ramakrishnan, M. Hyun, S. Y. Lee, M. He, J. Tucciarone, A. Selimbeyoglu, A. Berndt, L. Grosenick, K. A. Zalocusky, H. Bernstein, H. Swanson, C. Perry, I. Diester, F. M. Boyce, C. E. Bass, R. Neve, Z. J. Huang, K. Deisseroth, Targeting cells with single vectors using multiple-feature Boolean logic. *Nat. Methods* **11**, 763–772 (2014).
41. B. H. Weinberg, N. T. H. Pham, L. D. Caraballo, T. Lozano, A. Engel, S. Bhatia, W. W. Wong, Large-scale design of robust genetic circuits with multiple inputs and outputs for mammalian cells. *Nat. Biotechnol.* **35**, 453–462 (2017).
42. T. Kim, B. Weinberg, W. Wong, T. K. Lu, Scalable recombinase-based gene expression cascades. *Nat. Commun.* **12**, 2711 (2021).
43. A. E. Short, D. Kim, P. T. Milner, C. J. Wilson, Next generation synthetic memory via intercepting recombinase function. *Nat. Commun.* **14**, 5255 (2023).
44. S. E. Schindler, J. G. McCall, P. Yan, K. L. Hyrc, M. Li, C. L. Tucker, J. M. Lee, M. R. Bruchas, M. I. Diamond, Photo-activatable Cre recombinase regulates gene expression in vivo. *Sci. Rep.* **5**, 13627 (2015).
45. Y. Kuwasaki, K. Suzuki, G. Yu, Y. Kakiyama, M. Nishiwaki, K. Fushimi, R. Bekdash, Y. Shimizu, R. Narikawa, T. Nakajima, M. Yazawa, M. Sato, A semi-synthetic red light photoswitch for optogenetic control of protein activity. *Res. Sq.* 10.21203/rs.3.rs-450425/v1, (2021).
46. L. J. Bugaj, W. A. Lim, High-throughput multicolor optogenetics in microwell plates. *Nat. Protoc.* **14**, 2205–2228 (2019).
47. C. A. Lysiotis, L. L. Lairson, A. E. Boitano, H. Wurdak, S. Zhu, P. G. Schultz, Chemical control of stem cell fate and developmental potential. *Angew. Chem. Int. Ed. Engl.* **50**, 200–242 (2011).
48. W. Huang, E. Thokerunga, F. He, X. Zhu, Z. Wang, J. Tu, Regulatory of miRNAs in tri-lineage differentiation of C3H10T1/2. *Stem Cell Res. Ther.* **13**, 521 (2022).
49. D. C. Sloas, J. C. Tran, A. M. Marzilli, J. T. Ngo, Tension-tuned receptors for synthetic mechanotransduction and intercellular force detection. *Nat. Biotechnol.* **41**, 1287–1295 (2023).
50. A. M. Kabadi, P. I. Thakore, C. M. Vockley, D. G. Ousterout, T. M. Gibson, F. Guilak, T. E. Reddy, C. A. Gersbach, Enhanced MyoD-induced transdifferentiation to a myogenic lineage by fusion to a potent transactivation domain. *ACS Synth. Biol.* **4**, 689–699 (2015).
51. L. R. Polstein, M. Juhas, G. Hanna, N. Bursac, C. A. Gersbach, An engineered optogenetic switch for spatiotemporal control of gene expression, cell differentiation, and tissue morphogenesis. *ACS Synth. Biol.* **6**, 2003–2013 (2017).
52. D. Chakravarti, L. D. Caraballo, B. H. Weinberg, W. W. Wong, Inducible gene switches with memory in human T cells for cellular immunotherapy. *ACS Synth. Biol.* **8**, 1744–1754 (2019).
53. O. J. Noh, Y. H. Park, Y. W. Chung, I. Y. Kim, Transcriptional regulation of selenoprotein W by MyoD during early skeletal muscle differentiation. *J. Biol. Chem.* **285**, 40496–40507 (2010).
54. D. P. Murphy, T. Nicholson, S. W. Jones, M. F. O'Leary, MyoCount: A software tool for the automated quantification of myotube surface area and nuclear fusion index. *Wellcome Open Res.* **4**, 6 (2019).
55. J. Germán-Heins, M. Flury, Sorption of Brilliant Blue FCF in soils as affected by pH and ionic strength. *Geoderma* **97**, 87–101 (2000).
56. Y. Uda, Y. Goto, S. Oda, T. Kohchi, M. Matsuda, K. Aoki, Efficient synthesis of phycocyanobilin in mammalian cells for optogenetic control of cell signaling. *Proc. Natl. Acad. Sci. U.S.A.* **114**, 11962–11967 (2017).
57. V. Grishkevich, I. Yanai, Gene length and expression level shape genomic novelties. *Genome Res.* **24**, 1497–1503 (2014).
58. F. Chiaromonte, W. Miller, E. E. Bouhassira, Gene length and proximity to neighbors affect genome-wide expression levels. *Genome Res.* **13**, 2602–2608 (2003).
59. N. J. Kii, M. R. Snaith, J. A. Murray, Site-Specific recombinases: Tools for genome engineering. *Trends Genet.* **9**, 413–421 (1993).
60. A. Nagy, Cre recombinase: The universal reagent for genome tailoring. *Genesis* **26**, 99–109 (2000).
61. R. Kumar, A. K. Sharma, Transcription factor stoichiometry in cell fate determination. *J. Genet.* **100**, 27 (2021).
62. S. Takeda, J. P. Bonnamy, M. J. Owen, P. Ducey, G. Karsenty, Continuous expression of Cbfa1 in nonhypertrophic chondrocytes uncovers its ability to induce hypertrophic chondrocyte differentiation and partially rescues Cbfa1-deficient mice. *Genes Dev.* **15**, 467–481 (2001).
63. H. M. Blau, D. Baltimore, Differentiation requires continuous regulation. *J. Cell Biol.* **112**, 781–783 (1991).
64. A. Gelmi, C. E. Schutt, Stimuli-responsive biomaterials: Scaffolds for stem cell control. *Adv. Healthc. Mater.* **10**, e2001125 (2021).
65. S. Vanaei, M. S. Parizi, S. Vanaei, F. Saleemizadehpazari, H. R. Vanaei, An overview on materials and techniques in 3D bioprinting toward biomedical application. *Emg. Regen.* **2**, 1–18 (2021).
66. O. S. Thomas, M. Hörner, W. Weber, A graphical user interface to design high-throughput optogenetic experiments with the optoPlate-96. *Nat. Protoc.* **15**, 2785–2787 (2020).

**Acknowledgments:** We thank L. Gu for sharing his NanoReD plasmids and J. Ngo for sharing the MyoD plasmids. **Funding:** This work was supported by the National Institutes of Health [grants 1R01EB031904-01 (to W.W.W.), R01GM129011 (to W.W.W.), R01GM129011-S1 (to C.T.), TL1TR001410 (to I.K.), and F32HL160194 (to I.K.)] and the Paul Allen Foundation G-12963 (to W.W.W.). **Author contributions:** Conceptualization: C.T., I.K., and W.W.W. Data curation: C.T. Investigation: C.T., M.E.L.R., and J.D. Formal analysis: C.T. and J.D. Funding acquisition: C.T. and W.W.W. Methodology: C.T., I.K., and W.W.W. Project administration: C.T. and W.W.W. Resources: C.T. Software: C.T. and I.K. Supervision: C.T. and W.W.W. Validation: C.T., M.E.L.R., J.D., and W.W.W. Visualization: C.T. and W.W.W. Writing—original draft: C.T. and W.W.W. Writing—review and editing: C.T., I.K., and W.W.W. **Competing interests:** W.W.W. is a scientific cofounder and shareholder of Senti Biosciences and 4Immune. The other authors declare that they have no competing interests. **Data and materials availability:** The plasmids are available on Addgene. Source data are provided with this paper. All data needed to evaluate the conclusions in the paper are present in the paper and/or the Supplementary Materials.

Submitted 17 September 2024

Accepted 3 April 2025

Published 9 May 2025

10.1126/sciadv.adt1971